Title

Causal relationship between neuronal activity and cerebral hemodynamics in patients with ischemic stroke

Journal

Journal of Neural Engineering, 17(2)

ISSN

1741-2560

Authors

Wu, Dan
Liu, Xiuyun
Gadhoumi, Kais
et al.

Publication Date

2020-04-01

DOI

10.1088/1741-2552/ab75af

Peer reviewed

Published in final edited form as:

J Neural Eng. ; 17(2): 026006. doi:10.1088/1741-2552/ab75af.

Causal relationship between neuronal activity and cerebral hemodynamics in patients with ischemic stroke

Dan Wu, PhD[1,2,*], **Xiuyun Liu, PhD**[1,*], **Liping Liu, PhD**[3,4], **Kais Gadhoumi, PhD**[1], **Yuehua Pu, MD, PhD**[3,4], **Hemphill J. Claude**[5], **Zhe Zhang, MD, PhD**[3,4], **Xiao Hu, PhD**[1,6,7,8]

[1]Department of Physiological Nursing, University of California, San Francisco, USA

[2]School of Computer and Information Technology, Beijing Jiaotong University, Beijing, China

[3]Neurointensive Care Unit, Department of Neurology, Beijing Tiantan Hospital, Capital Medical University, Beijing, China

[4]China National Clinical Research Center for Neurological Diseases, Beijing Tiantan Hospital, Capital Medical University, Beijing, China

[5]School of Medicine, University of California, San Francisco, USA

[6]Department of Neurosurgery, School of Medicine, University of California, Los Angeles, USA

[7]Department of Neurological Surgery, University of California, San Francisco, USA

[8]Institute of Computational Health Sciences, University of California, San Francisco, USA

Abstract

Objective.—Neurovascular coupling enables rapid adaptation of cerebral blood flow (CBF) to support neuronal activity. Modern techniques enable the simultaneous recording of neuronal activities and hemodynamic parameters. However, the causal relationship between electrical brain activity and CBF is still unclarified. In this study, we investigated the causal relationship between surface electroencephalogram (EEG) and cerebral blood flow velocity (FV) from transcranial Doppler(TCD) using Granger causality (GC) analysis.

Approach.—Twenty simultaneous recordings of EEG and FV from 17 acute ischemic stroke patients were studied. Each patient had simultaneous, continuous monitoring of EEG and bilateral FVs in either the middle cerebral arteries (MCA) or posterior cerebral arteries (PCA). The causal interactions between FV (0.006 – 0.4 Hz) and EEG (delta, theta, alpha, beta and gamma bands) were investigated through GC index (GCI). In order to make the GCIs comparable, the proportion of GCI (PGCI) values where G-causality is statistically significant were calculated. Scores on the NIH Stroke Scale (NIHSS) and the modified Rankin Scale (mRS) for neurologic disability were recorded respectively at discharge. Patients were divided into a deceased (mRS = 6) and a survival group (mRS = 1 to 5), and a favorable (mRS: 1 to 2) and unfavorable outcome group (mRS: 3 ~ 6).

Corresponding author: Xiao Hu, Department of Physiological Nursing, 2 Koret Way, University of California, San Francisco, CA, 94143, USA. xiao.hu@ucsf.edu.

*Share the same first authorship

Main Results.—This study identified a causal relationship from EEG → FV, indicating EEG contained information that can be used for FV prediction. PGCI was negatively related with mRS ($p<0.05$), indicating that stronger causalities between EEG and FV exist in patients with better outcome. The NIHSS was negatively related with the asymmetry of the two-side PGCI, calculated as the difference between the lesional side and non-lesional side PGCI.

Significance.—A causal relationship from EEG → FV may exist in patients with ischemic stroke. The strength of G-causality may be related to stroke severity at discharge.

Keywords

Neurovascular Coupling; Granger Causality; EEG; Cerebral Blood Flow; Stroke

Introduction

Electroencephalography (EEG) has been widely used as a noninvasive tool to study epilepsy, cognitive function, and assess brain states in humans since Berger first reported alpha rhythm (1). EEG has also been extensively used in the delineation of subclinical brain injuries during neurosurgical procedures (2) and to inform about stroke features and prognosis (3). Timely detection of brain ischemia is critical to prevent secondary injuries (4) and monitoring techniques are needed to aid in this diagnosis. It has been recognized that a close relationship exists between electrical brain activities — measured with EEG — and hemodynamic responses — measured with functional magnetic resonance imaging (fMRI) (5–7). Modulations in alpha rhythms are known to be negatively correlated with modulations on blood oxygen level dependent (BOLD) fMRI (7). However, clarifying the neurophysiology of hemodynamic responses has been hindered by the limited temporal resolution of fMRI (8). Transcranial Doppler ultrasonography (TCD) is a non-invasive technique that assesses blood flow velocity (FV) in large cerebral arteries (9), which is inexpensive, portable and safe. Its high temporal resolution allows investigation of changes in cerebral hemodynamics and neuronal dynamics in a time-synched fashion. Lam et al. (10) demonstrated that the onset of electrocerebral silence recorded on EEG is associated with a sudden reduction of cerebral blood flow velocity. Martynova et al. (11) reported a significant correlation between EEG spectral distribution and FV in coronary arteries of stroke patients. Interestingly, some researchers found significant correlation between FV and EEG (2,12) while others did not (13–15). Of note, these studies mostly used correlation or coherence to measure the statistical (linear) relationship between FV and EEG. However, these measures do not provide insight into the directionality of information flow between electrical brain activities and hemodynamic responses (16).

In a normal physiological state, it is expected that neuronal activities increase metabolism and then CBF. Therefore, neurovascular coupling has an inherence directionality. However, invasive studies using electrocorticographic (ECoG) and laser Doppler flowmetry to measure local CBF have identified paradoxical decrease of CBF when patients develops cortical spreading depolarization (17,18). Also, it is known that abnormal EEG patterns emerge when CBF dropped below critical level (8,19), indicating a reversed causal relationship. Therefore, adopting approaches of analyzing EEG and FV that can reveal direction of

causality would enrich the information to be derived from these two signals and more comprehensively characterize the state of neurovascular coupling.

In the present study, we analyzed the causal relationship between continuous EEG and FV recordings using a widely used methodology, Granger causality (GC), which was first introduced by Norbert Wiener in 1956(20), and further developed in 1969 by the econometrician Clive Granger (21). To our knowledge, this is the first study to assess causal relationship between EEG and FV. Signals were collected from a cohort of patients with ischemic stroke post intravenous injection of tissue plasminogen activator (IV-tPA) or thrombectomy to whom multimodality monitoring were applied as part of a research protocol to study its potential in providing decision support with regard to blood pressure management and early detection of patient deterioration. Towards that goal, we further elucidate the clinical relevance of neurovascular coupling characteristics by studying the relationships between the strength of causality and two clinical scores, the NIH Stroke Scale score (NIHSS) and the modified Rankin Scale (mRS) score.

Methods

2.1 Subjects and data sampling

Twenty recordings from seventeen ischemic stroke patients (three females) admitted to the Neurointensive Care Unit (Department of Neurology, Beijing Tiantan Hospital, Capital Medical University, Beijing, China) were studied. The mean age of the patients enrolled in the study was 61.6 ± 10.3 years. Three patients were monitored twice on the 2^{nd} and 4^{th} day after admission (patient 7, 11 and 15). All other patients were monitored once. Each recording lasted between 15 and 175 minutes. The patients were treated with IV-tPA within 6 hours after stroke symptoms begin or with embolectomy if admitted after 6-hour window. The recanalization was verified using computed tomography angiography (CTA) or magnetic resonance angiography (MRA) after 24-hour surgery. Inclusion criteria were: (1) age ≥18 years; (2) acute ischemic stroke confirmed by computed tomography (CT) or magnetic resonance imaging (MRI); (3) stroke onset within 24 hours prior to hospital admission; (4) stroke caused by cerebral large artery occlusion, including internal carotid artery (ICA), middle cerebral artery (MCA), and vertebral or basilar artery (BA). We excluded patients who had an insufficient or absent acoustic temporal bone window for TCD FV recording or who had scalp wounds or infections preventing EEG electrode placement.

All enrolled patients underwent simultaneous, continuous monitoring of 8-lead EEG, noninvasive arterial blood pressure (ABP), and TCD FV of the bilateral MCA or posterior cerebral arteries (PCA). Written consent was obtained from each patient or the next of kin. The study was approved by the local Institutional Review Board (IRB). Scores on the NIHSS and mRS were recorded at discharge.

We monitored bilateral FVs from the MCA for the anterior circulation stroke patients (n = 14) and FVs from PCA (n = 3) for posterior circulation stroke patients through 2-MHz probes mounted on a headband using transcranial Doppler ultrasound (Doppler BOX, DWL, Singen, Germany or EMS-9PB Transcranial Doppler Ultrasound System, Delica, China). ABP was continuously monitored through noninvasive finger plethysmography (CNAP

Monitor 500, Graz, Austria or Finometer model 1, Finapres, Netherlands). Continuous EEG monitoring was performed using 8 electrodes placed according to the international 10–20 system. EEG recordings were acquired using a Nicolet system (Nicolet V44 EEG Monitor, Natus Neurology Incorporated, Wisconsin, USA or NSD-7101 Neuro Monitor System, Delica, China) and analyzed in a longitudinal bipolar montage (F3-C3, T3-P3, P3-O1, F4-C4, T4-P4, P4-O2) (22). FV and ABP recordings were recorded simultaneously with EEG signals through the neuro monitoring system (Nicolet V44 EEG Monitor or NSD-7101 Neuro Monitor System) at a sampling frequency of 500 Hz.

2.2 Data processing

As a preprocessing step, the first author reviewed all the data and removed all the data with losing channels or obvious artifact (electromyography and electrooculography). Data from each EEG and FV channel were normalized by subtracting the mean value and dividing by the standard deviation of values across that channel. Bilateral FV signals were filtered using a band pass filter (Chebyshev Type II filter, 0.0055–0.4Hz) with the lower frequency limit corresponding to the lower frequency of the so called “B” waves in cerebral hemodynamic signals including CBFV (23). EEG recordings were notch-filtered to remove line noise and band-pass filtered between 0.5 and 70 Hz. Hilbert transformation was applied to extract instantaneous amplitudes in 5 frequency bands of the EEG signals (delta (0.5–4 Hz), theta (47Hz), alpha (7–13 Hz), beta (13–30 Hz) and gamma (30–45 Hz). The stationarity of the EEG and FV series was tested by Augmented Dickey-Fuller test for unit root, and the results showed the series after normalization were stationary. A GC index (see section 2.3) was calculated to estimate the causal relationship between FV and instantaneous EEG amplitude in fifty 5-min windows randomly selected (bootstrapping method) without avoiding overlapping of selected windows in each recording.

2.2.1 Instantaneous EEG Amplitude Calculation—

Hilbert transformation leads to a complex signal representation from which the phase, energy, and (instantaneous) frequency can be derived (24–26). Let v_t be a representation of an EEG channel and its complex representation V_t can be defined as:

$$V_t = v_t + iv'_t \tag{1}$$

where imaginary signal v'_t is given by the Hilbert transform of v_t:

$$v'_t = \frac{1}{\pi} PV \int_{-\infty}^{\infty} \frac{v_\tau}{t-\tau} d\tau = -\frac{1}{\pi} \lim_{\epsilon \to 0} \int_{\epsilon}^{\infty} \frac{v'_t - v_{t-\tau}}{\tau} d\tau \tag{2}$$

where PV is the Cauchy Principal value. At any given time point, the instantaneous amplitude A_t of an EEG signal v_t can be calculated as the analytic amplitude of the complex vector V_t, namely:

$$A_t = \sqrt{|v_t|^2 + |v'_t|^2} \tag{3}$$

2.2.2 Determination of EEG and FV directional information based on Granger causality—A signal Y is said to Granger-cause (G-cause) a signal X when the knowledge of past information in X and Y improves the prediction of X in comparison with the knowledge of past information of X alone (16). Assuming two autoregressive (AR) models of a signal X_t as follows:

$$X_t = \sum_{i=1}^{m} a_i X_{t-i} + \varepsilon_t \tag{4}$$

$$X_t = \sum_{i=1}^{m} a_i X_{t-i} + \sum_{i=1}^{m} b_i Y_{t-i} + \varepsilon'_t \tag{5}$$

where m is the model order, a_i and b_i are the parameters, ε_t and ε'_t are the residual of the models. To evaluate if G-causality exists between signals X and Y, we can determine which of the models in eq. (4) and (5) better fits the underlying data. The G-causality between X and Y ($G_{Y\to X}$) can then be estimated using:

$$G_{Y\to X} = \ln\frac{var(\varepsilon_t)}{var(\varepsilon'_t)}, \quad G_{Y\to X} > 0 \tag{6}$$

$G_{Y\to X}$ is a measure of the strength of G-causality between X and Y. The larger $G_{Y\to X}$ is, the better the bivariate model in eq. (5) fits the data than the model in eq. (4) is, and the stronger the G-causality between Y and X is (where Y G-causes X). The statistical significance of an F-test comparing the goodness of fit of each model can be used as an estimate of the strength of G-causality between X and Y. The F-statistic in this case is given by:

$$F = \frac{between-models\ variability}{within-models\ variability} = \frac{\frac{RSS_X - RSS'_X}{m}}{\frac{RSS'_X}{T-2m-1}} \tag{7}$$

where RSS_X and RSS'_X are the Residual Sum of Squares of the models of equation (4) and equation (5), respectively and T is the number of observations used to estimate the *bivariate* model in equation (5). Here, the F-statistic approximately follows an F distribution with degrees of freedom m and (T-2m-1) under the null hypothesis. The Bayesian information Criterion was used to select the best order m with a maximum order of m = 15 (no down-sampling was applied).

We hereafter define a Granger Causality Index (GCI) between EEG and FV as the F-value derived in equation (7) with X and Y representing respectively EEG and FV signals. GCI estimates a directional G-causality and hence will be denoted as $GCI_{EEG\to FV}$ and $GCI_{FV\to EEG}$, respectively. We calculate GCI in 5-min windows, between the 6 EEG channels and bilateral FV channels. The start of each window was obtained randomly for each recording. In total, 50 GCI values were calculated for each recording, regardless the different length of each recording. The distribution of these time-window was showed in Supplementary Figure 1. The range of GCI values varies between different channels and

different patients, therefore, in order to make the GCIs comparable, we calculated the proportion of GCI (PGCI) values where G-causality is statistically significant, based on the critical value of F-distribution ($p = 0.05$), out of the 50 random windows described above (see section 2.5) for subsequent statistical analysis.

2.4 Surrogate data

In order to validate the causal relationship that was found in this study, we also created a cohort of surrogate data through Monte Carlo simulation. The surrogate data were generated by destroying the phase relationship in the original recordings. For each 5-min segment of EEG and FV recordings, a fast Fourier transform (FFT) was calculated to acquire the phase of the signal which we then changed using a random order. The phase-destructed signal was then transformed back into the temporal domain using an inverse fast Fourier transform (IFFT). Fifty 5-min surrogate windows were generated for each recording in the following way. When we test the null hypothesis of the existence of G-causality from EEG to FV, we use surrogate EEG (sEEG) and raw FV (rFV). When the null hypothesis is the existence of G-causality from FV to EEG, we use surrogate FV (sFV) and raw EEG (rEEG). In this way, the accuracy of using only historical data from the hypothesized driven signal will not be affected but any potential predictive power of the driving signal is destroyed in the surrogate data.

2.5 Statistical analysis

$GCI_{EEG \rightarrow FV}$ and $GCI_{FV \rightarrow EEG}$ were estimated in five EEG frequency bands. For each 5-minute segment, 60 [2 (*FV*) × 6(*EEG channels*) × 5(*EEG frequency bands*] GCI values were calculated for each direction. We compared the proportion of 5-minute windows with significant G-causality in both directions using a Wilcoxon rank sum test (as PGCIs are not normally distributed) to estimate the dominant direction of G-causality and applied the same statistical comparison to surrogate data.

Since the causality from EEG to FV direction is stronger than the opposite direction, the PGCI from EEG to FV direction was used for the following analysis. Two-way repeated measures ANOVA was used to investigate the effect of channel laterality and frequency bands, and the interaction between channels and frequency bands. If no interaction effect exists between the two factors and if a main effect was observed (i.e. p value < 0.05), a multiple comparison test (LSD) was used to identify the channels or frequency bands with a statistically significant difference.

In this study, we monitored bilateral FVs (left and right side TCD), and bilateral EEG signals (Left side: F3-C3, T3-P3, P3-O1; Right side: F4-C4, T4-P4, P4-O2). The GCI pair from the same side, e.g. left FV and F3-C3, was defined as ‘ipsilateral’; and the pair from different sides, e.g. left FV and F4-C4, was named ‘contralateral’. Since the variable in question is not normally distributed, the non-parametric Wilcoxon rank sum test was used to investigate the difference between ipsilateral and contralateral channel pairs.

Patients were divided into a deceased (mRS = 6) and a survival group (mRS = 1 to 5), and into a favorable (mRS: 1 to 2) and unfavorable outcome group (mRS: 3 ~ 6) (27). A two-way ANOVA (repeated measures), including within-subject factor (EEG frequency bands)

and between-subjects factor (mRS groups), was carried out to test the null hypothesis that there are no significant differences of PGCI in these two subgroups and frequency bands. Patients were also divided into three subgroups according to NIHSS at discharge: NIHSS < 10, 10 ≤ NIHSS < 20 and NIHSS ≥ 20. A two-way ANOVA (repeated measures) was carried out to test the null hypothesis that there are no significant differences of mean GCI in these three subgroups and the frequency bands. The correlation between PGCI and mRS and between PGCI and NIHSS at discharge was assessed using Spearman's rank correlation. Each channel was calculated in all the five EEG frequency bands. The average and bilateral difference ($PGCI_{lesional}$ - $PGCI_{non\text{-}lesional}$) were also used for the correlation estimation. The lesional information of each subject was showed in Table 1, and the subjects with "BA" were excluded in bilateral difference analysis.

Results

3.1 Patient demographics.

Information about each patient's stroke lesion territory, age, NIHSS and mRS at discharge are summarized in Table 1. The mean duration of the twenty recordings is 101.8 ± 42.2 minutes, ranging from 15 to 175 minutes.

3.2 Causal relationship between EEG and FV

Figure 1 shows an example of GCI values of a patient (90-minute recording). GCI varies between and within EEG channels across the whole recording period, indicating a dynamic causal relationship between EEG and FV.

Figure 2 shows the percentage of significant GCI recording for each patient (one row is one recording, with red color indicating high PGCI and blue color indicating low PGCI). Proportions with significant G-causality in the direction EEG→FV were found to be significantly higher in all patients comparing with the proportions from the direction of FV→EEG (Wilcoxon rank sum test; $p < 0.01$, see Fig. 2 and Table 2).

The GCI values using surrogate data (green and red bars in Figure 3) were significantly lower than GCI values using original data (blue bar, Fig 3) in the direction of EEG → FV. However, there was no significant difference between GCI using surrogate data and original data in the direction of FV → EEG (Wilcoxon rank sum test, $p > 0.05$).

3.3 Influence of EEG frequency bands and EEG channels

Two-way ANOVA (repeated measures) was used to investigate whether PGCI values varied with EEG channels and/or EEG frequency bands (20 recordings). A main effect exists with frequency bands ($p = 0.01$), but not with EEG channels ($p = 0.283$). No interaction effect exists between the two factors ($p = 0.801$). Multiple comparison test (LSD) showed that the PGCI in beta band (mean ± SD: 0.824 ± 0.01) was significantly lower than in delta band (0.843±0.01, $p = 0.026<0.05$), theta band (0.848 ± 0.01, $p = 0.017<0.05$) and in alpha band (0.847± 0.009, $p = 0.018<0.05$). PGCI in gamma band (0.832±0.012) was significantly lower than in theta ($p = 0.001<0.05$) and alpha band ($p = 0.017<0.05$). There were no

significant differences between the average PGCI values of the ipsilateral and contralateral EEG and FV channels.

3.4 Correlation with clinical outcome

The EEG frequency bands showed main effects ($p = 0.019$), while the patient outcome (deceased/survival, $p = 0.187$ or unfavorable/favorable outcome, $p = 0.336$) showed no significant differences. There was no interaction effect among these factors. There was a significant correlation between PGCI and mRS at discharge in most channels and frequency bands, including delta, theta, alpha and gamma (Table 3).

Figure 4 shows a statistically significant negative linear relationship between mRS and PGCI in the delta band ($R = -0.71$, $p = 0.00$), theta ($R = -0.59$, $p = 0.02$), alpha ($R = -0.59$, $p = 0.02$), beta ($R = -0.57$, $p = 0.03$) and gamma ($R = -0.62$, $p = 0.01$).

The two-way repeated measures ANOVA was conducted to compare the PGCI in the within-subject factor (EEG frequency bands) and the between-subject factor (the NIHSS group). There was a main effect in EEG frequency bands ($p = 0.01<0.05$), but no significant difference exists among the NIHSS groups. There was no interaction effect among these factors. Table 4 shows the correlation between PGCI and NIHSS at discharge.

Figure 5 shows a significant relationship between discharge NIHSS and the PGCI bilateral difference in the delta band ($R = -0.68$, $p = 0.01$), and the other bands had no significant relationship.

Discussion

In this study we demonstrated again the feasibility and clinical potential of analyzing simultaneously recorded spontaneous EEG and cerebral blood flow velocity signals to characterize neurovascular coupling. In our previous study(28), the phase of slow wave of FV in the MCA was found to entrain the amplitude of EEG from the occipital region in beta and gamma frequency bands. The present study utilizes a different technique that focuses more on the amplitude changes in both signals. In contrast to the previous technique, GC analysis can provide an estimate of the directionality of the coupling. The results obtained support the physiologically plausible notion that neuronal activity precedes cerebral hemodynamic changes. This finding was also previously reported by Lam and Simpson (10,29) who demonstrated that EEG changes preceded CBF changes by about 5–7 seconds. However, the results from the present and our previous study also imply that neurovascular coupling characteristics are multi-faceted and can be reflected in different ways in which how EEG and FV interact. Further work should investigate whether the phenomenon seen in this study of patients with ischemic stroke occurs in other pathological conditions that involve different types of brain injury.

Neurovascular coupling, the intrinsic regulative mechanism that rapidly adjusts local cerebral blood flow (3) to follow the changes in neuronal activity, is one of the key functions involved in preserving cerebral blood supply to the brain and preserving the normal function of the brain. Despite the importance of this phenomenon, there has been limited research

regarding development of techniques to monitor this at the bedside in the neurocritical care setting. In contrast, pressure autoregulation (30–32) has been widely studied, perhaps because intracranial pressure and arterial blood pressure are more routinely monitored while EEG and TCD are used less often, especially as continuous and concurrent monitors. Therefore, another key contribution of the present and our previous study is an illustration of using EEG and FV, both of which can be noninvasively collected, to potentially monitor neurovascular coupling status at the bedside to inform clinical decisions of managing patients with brain injuries.

It should be also noted that surrogate data analysis is a necessary technique. As shown in our results (Fig 3), statistically significant GCI (based on F-statistics) can often be obtained when using a phase-scrambled surrogate data as a driving signal when the driven signal is readily predicted from its own historical values. In our case, more than 70% of sEEG→rFV show statistically significant GCI. Therefore, relying on F-statistics would have drawn the conclusion that surrogate EEG granger causes FV - which is an erroneous conclusion. However, Fig.3 shows the GCI of EEG→FV is clearly larger than that of sEEG→FV, which provides more convincing evidence that EEG Granger causes FV. In the same figure, we also observe that there is no difference between FV→EEG and sFV→EEG and hence surrogate data analysis also helps reject the notation that FV could Granger cause FV.

The correlation between mRS and PGCI indicates patients with milder initial insult, and possibly better outcome, tend to have a more robust cerebral hemodynamic response to changes in EEG. This may be representative of intact microvascular autoregulation or indicate a protective effect of intact neurovascular coupling. Another potential reason for low correlation in the more severely affected patients is lower variability of EEG envelopes. When the dispersion of the data decreases, the correlation is also likely to decrease because the unexplained random variation in FV becomes relatively more important. Previous studies already showed that EEG power is markedly affected in stroke patients with a significant increase in Delta power (1–4 Hz) accompanied by a decrease in Alpha (8–14 Hz) and Beta (14–30 Hz) power (33,34). The increasing power of slow rhythms and decreasing power of fast rhythms are directly linked with neuronal metabolism and reflect ischemic injury (8). The decreased variability of EEG in alpha and beta bands in severe patients may be the reason of lower GCI. Further research with larger cohorts of patients and a different design of data collection schema (e.g., sequential recording of EEG and FV throughout a patient’s stay in the neurocritical unit) are needed to further validate this result.

Limitation

The Granger causality analysis carried out in this work is based on linear regression models and stationary signals. Nonlinear causality methods may offer better tools to assess nonlinear causal relationships that might exist between EEG and FV. Another limitation of this study is the relatively poor spatial coverage of brain regions due to the limited number of available EEG channels. It will be interesting to examine if the observed neurovascular causality can be better delineated with higher density EEG recordings (e.g. 21 or more channels). This type of setup could shed more detailed light on areas of the brain with the strongest causality and potentially elucidate new mechanisms of neurovascular functional

dynamics and their disruption by stroke and other neurological insults. Moreover, anesthetic state of patients may also influence the EEG and cerebral blood flow. However, due to the retrospective nature of this study, we did not record the details of anesthetic drugs that we gave to these patients. We should record these information in the future study.

Conclusion

Changes in FV are G-caused by EEG changes in patients with ischemic stroke and NIHSS at discharge is negatively correlated with the strength of this G-causality.

Supplementary Material

Refer to Web version on PubMed Central for supplementary material.

Acknowledgements

The algorithm and data analysis portion of this project work was partially supported by the Middle Career Scientist Award, the UCSF Institute for Computational Health Sciences, the National Institutes of Health Awards (NS106905A1). The data collection and clinical interpretation of results were partially funded by the Fundamental Research Funds for the Central Universities in China (2016RC022) and the National Natural Science Foundation of China (61773048).

References

1. Tarantini S, Tran CHT, Gordon GR, Ungvari Z, Csiszar A. Impaired neurovascular coupling in aging and Alzheimer's disease: Contribution of astrocyte dysfunction and endothelial impairment to cognitive decline. Vol. 94, Experimental Gerontology. 2017. p. 52–8. [PubMed: 27845201]
2. Rosengarten B, Huwendiek O, Kaps M. Neurovascular coupling and cerebral autoregulation can be described in terms of a control system. Ultrasound Med Biol. 2001;27(2):189–93. [PubMed: 11316527]
3. Fritzsch C, Rosengarten B, Guschlbauer B, Weiller C, Hetzel A, Reinhard M. Neurovascular coupling and cerebral autoregulation in patients with stenosis of the posterior cerebral artery. J Neuroimaging. 2010;20(4):368–72. [PubMed: 19732298]
4. Girouard H. Neurovascular coupling in the normal brain and in hypertension, stroke, and Alzheimer disease. J Appl Physiol [Internet]. 2006;100(1):328–35. Available from: http://jap.physiology.org/cgi/doi/10.1152/japplphysiol.00966.2005
5. Franceschini MA, Radhakrishnan H, Thakur K, Wu W, Ruvinskaya S, Carp S, et al. The effect of different anesthetics on neurovascular coupling. Neuroimage. 2010;
6. Chen Y, Xu W, Wang L, Yin X, Cao J, Deng F, et al. Transcranial Doppler combined with quantitative EEG brain function monitoring and outcome prediction in patients with severe acute intracerebral hemorrhage. Crit Care. 2018;
7. Sharbrough FW, Messick JM, Sundt TM. Correlation of continuous electroencephalograms with cerebral blood flow measurements during carotid endarterectomy. Stroke. 1973;4(4):674–83. [PubMed: 4723697]
8. Foreman B, Claassen J. Quantitative EEG for the detection of brain ischemia. Vol. 16, Critical Care. 2012.
9. Purkayastha S, Sorond F. Transcranial doppler ultrasound: Technique and application. Semin Neurol. 2012;32(4):411–20. [PubMed: 23361485]
10. Lam AM, Matta BF, Mayberg TS, Strebel S. Change in cerebral blood flow velocity with onset of EEG silence during inhalation anesthesia in humans: Evidence of flow-metabolism coupling? J Cereb Blood Flow Metab. 1995;

11. Martynova OV, Portnova GV, Gladun KV Neural correlates of brain state in chronic ischemia and stroke: Combined resting state electroencephalogram and transcranial Doppler ultrasonographic study. Neuroreport. 2017;
12. Szirmai I, Amrein I, Pálvölgyi L, Debreczeni R, Kamondi A. Correlation between blood flow velocity in the middle cerebral artery and EEG during cognitive effort. Cogn Brain Res. 2005;
13. Jeong I, Lee H, Kim S. Cerebral Blood Flow Velocity and Eeg Response during Ergometer Exercise in Normoxia and Hypoxia. Med Sci Sport Exerc. 2018;50(55):332.
14. Lagerlund TD, Low PA, Novak V, Novak P, Hines SM, McPhee B, et al. Spectral analysis of slow modulation of EEG amplitude and cardiovascular variables in subjects with postural tachycardia syndrome. Auton Neurosci Basic Clin. 2005;
15. Melamed E, Lavy S, Portnoy Z, Sadan S, Carmon A. Correlation between regional cerebral blood flow and EEG frequency in the contralateral hemisphere in acute cerebral infarction. J Neurol Sci. 1975;26(1):21–7. [PubMed: 1159456]
16. Hesse W, Möller E, Arnold M, Schack B. The use of time-variant EEG Granger causality for inspecting directed interdependencies of neural assemblies. J Neurosci Methods. 2003;
17. Dreier JP, Major S, Manning A, Woitzik J, Drenckhahn C, Steinbrink J, et al. Cortical spreading ischaemia is a novel process involved in ischaemic damage in patients with aneurysmal subarachnoid haemorrhage. Brain. 2009;
18. Dreier JP, Woitzik J, Fabricius M, Bhatia R, Major S, Drenckhahn C, et al. Delayed ischaemic neurological deficits after subarachnoid haemorrhage are associated with clusters of spreading depolarizations. Brain. 2006;
19. Jordan KG. Emergency EEG and Continuous EEG Monitoring in Acute Ischemic Stroke. J Clin Neurophysiol. 2004;
20. Wiener N. The theory of prediction. In: Modern mathematics for the engineer, editor Beckenbach EF. 1956.
21. Granger CWJ. Investigating Causal Relations by Econometric Models and Cross-spectral Methods. Econometrica. 1969;
22. Alotaiby T, El-Samie FEA, Alshebeili SA, Ahmad I. A review of channel selection algorithms for EEG signal processing. EURASIP J Adv Signal Process. 2015;
23. Spiegelberg A, Preuß M, Kurtcuoglu V. B-waves revisited. Interdiscip Neurosurg Adv Tech Case Manag. 2016;6:13–7.
24. Demirer RM, Ozerdem MS, Bayrak C. Classification of imaginary movements in ECoG with a hybrid approach based on multi-dimensional Hilbert-SVM solution. J Neurosci Methods. 2009;
25. Demirer RM, Özerdem MS, Bayrak C, Mendi E. Determination of ECoG information flow activity based on Granger causality and Hilbert transformation. Comput Methods Programs Biomed. 2013;
26. Freeman WJ, Burke BC, Holmes MD. Aperiodic phase re-setting in scalp EEG of beta-gamma oscillations by state transitions at alpha-theta rates. Hum Brain Mapp. 2003;
27. Sato S, Uehara T, Ohara T, Suzuki R, Toyoda K, Minematsu K. Factors associated with unfavorable outcome in minor ischemic stroke. Neurology. 2014;
28. Liu X, Pu Y, Wu D, Zhang Z, Hu X, Liu L. Cross-Frequency Coupling Between Cerebral Blood Flow Velocity and EEG in Ischemic Stroke Patients With Large Vessel Occlusion. Front Neurol [Internet]. 2019; Available from: 10.3389/fneur.2019.00194
29. Simpson DM, Infantosi AFC, Botero Rosas DA. Estimation and significance testing of cross-correlation between cerebral blood flow velocity and background electro-encephalograph activity in signals with missing samples. Med Biol Eng Comput. 2001;
30. Panerai RB. Cerebral autoregulation: From models to clinical applications. Vol. 8, Cardiovascular Engineering. 2008. p. 42–59. [PubMed: 18041584]
31. Czosnyka M, Smielewski P, Piechnik S, Steiner L a, Pickard JD. Cerebral autoregulation following head injury. J Neurosurg. 2001;95(5):756–63. [PubMed: 11702864]
32. Liu X, Czosnyka M, Donnelly J, Budohoski KP, Varsos GV, Nasr N, et al. Comparison of frequency and time domain methods of assessment of cerebral autoregulation in traumatic brain injury. J Cereb Blood Flow Metab. 2014;11(October):1–9.
33. Faught E. Current role of electroencephalography in cerebral ischemia. Stroke. 1993.

34. Lu XCM, Williams AJ, Tortella FC. Quantitative electroencephalography spectral analysis and topographic mapping in a rat model of middle cerebral artery occlusion. Neuropathol Appl Neurobiol. 2001;

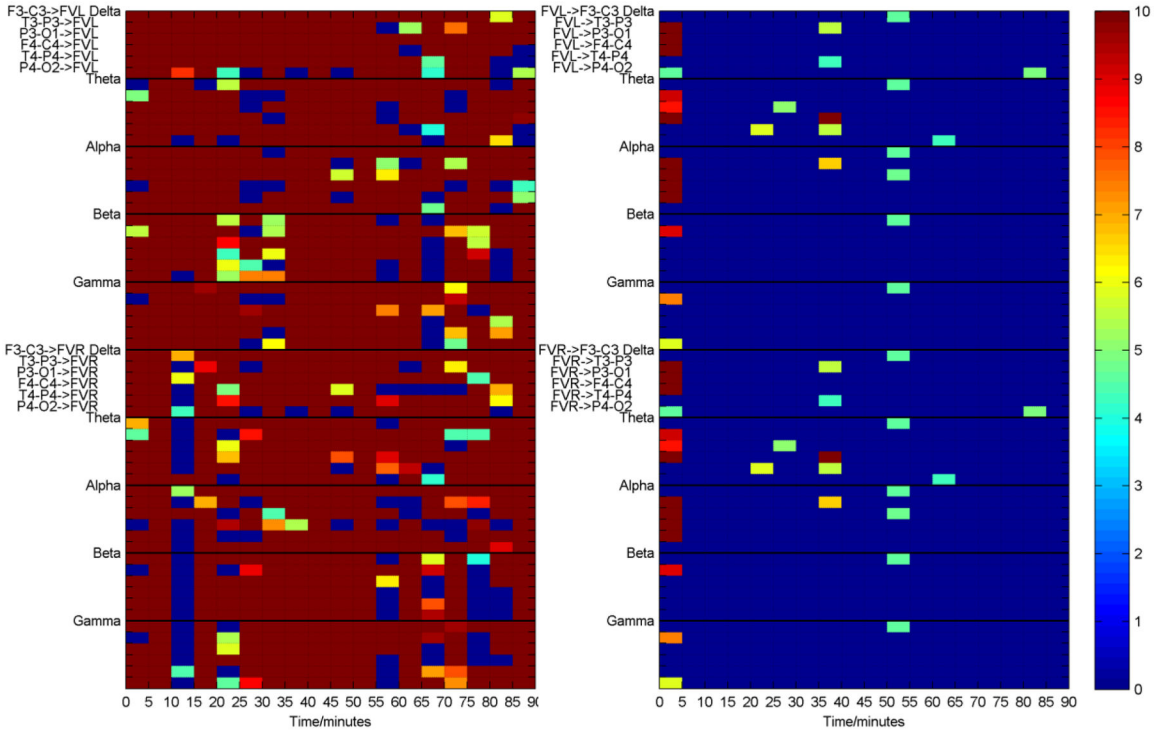

Figure 1.

Granger causality Index (GCI) in patient 1, calculated in a 90-minute recording. y-axis shows GCI values for the indicated pair of EEG and FV channels in 5 EEG frequency bands. In order to improve the visualization of this graph, the GCI values were rescaled between 0 and 10, which means GCI above 10 was made 10.

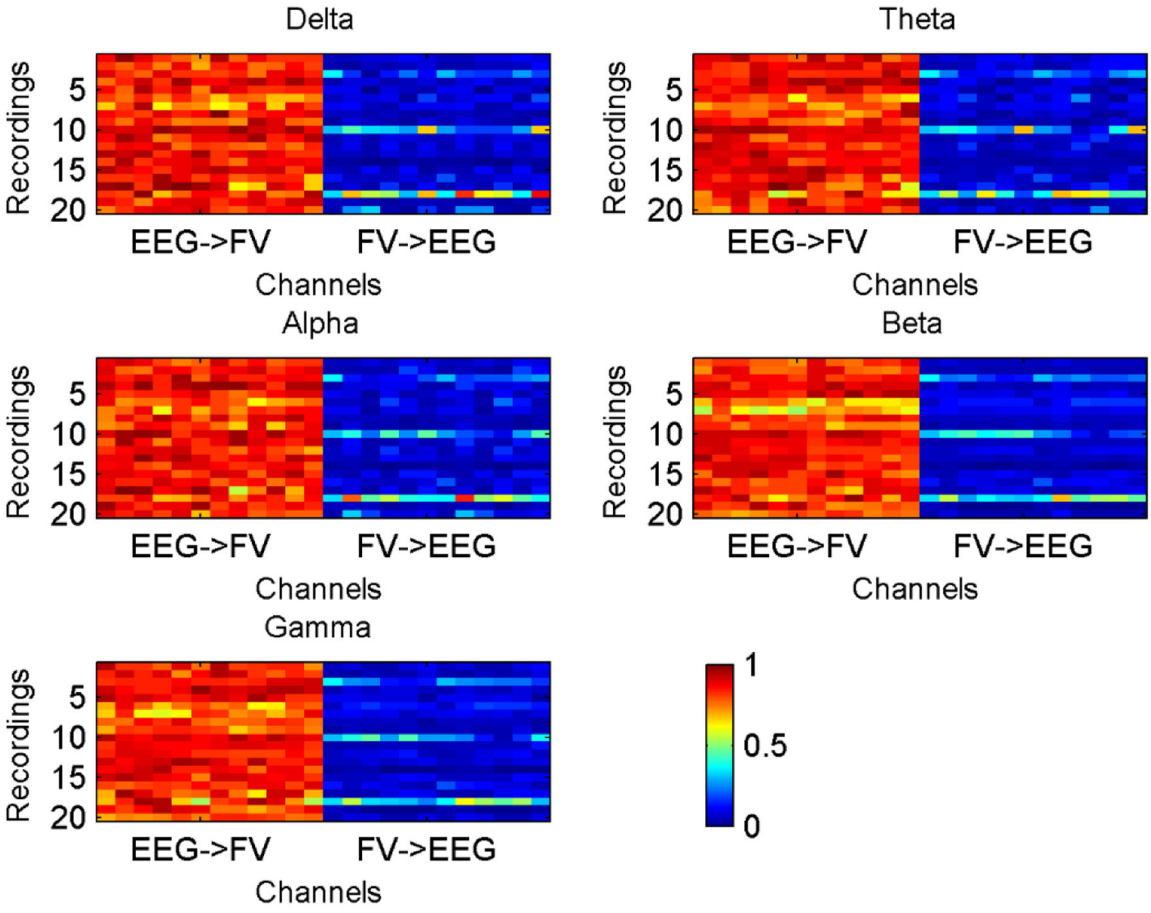

Figure 2.

Proportions of 5-minute windows showing statistically significant GCI for each recording (n = 20). Each subgraph represents the proportion with significant G-causality in a given EEG band. Each row represents one recording. The right and left panels of each box show the average (across 6 EEG channels and bilateral FV channels) proportions in the EEG→FV and in the FV→EEG respectively. GCI: Granger causality Index. FV: cerebral blood flow velocity.

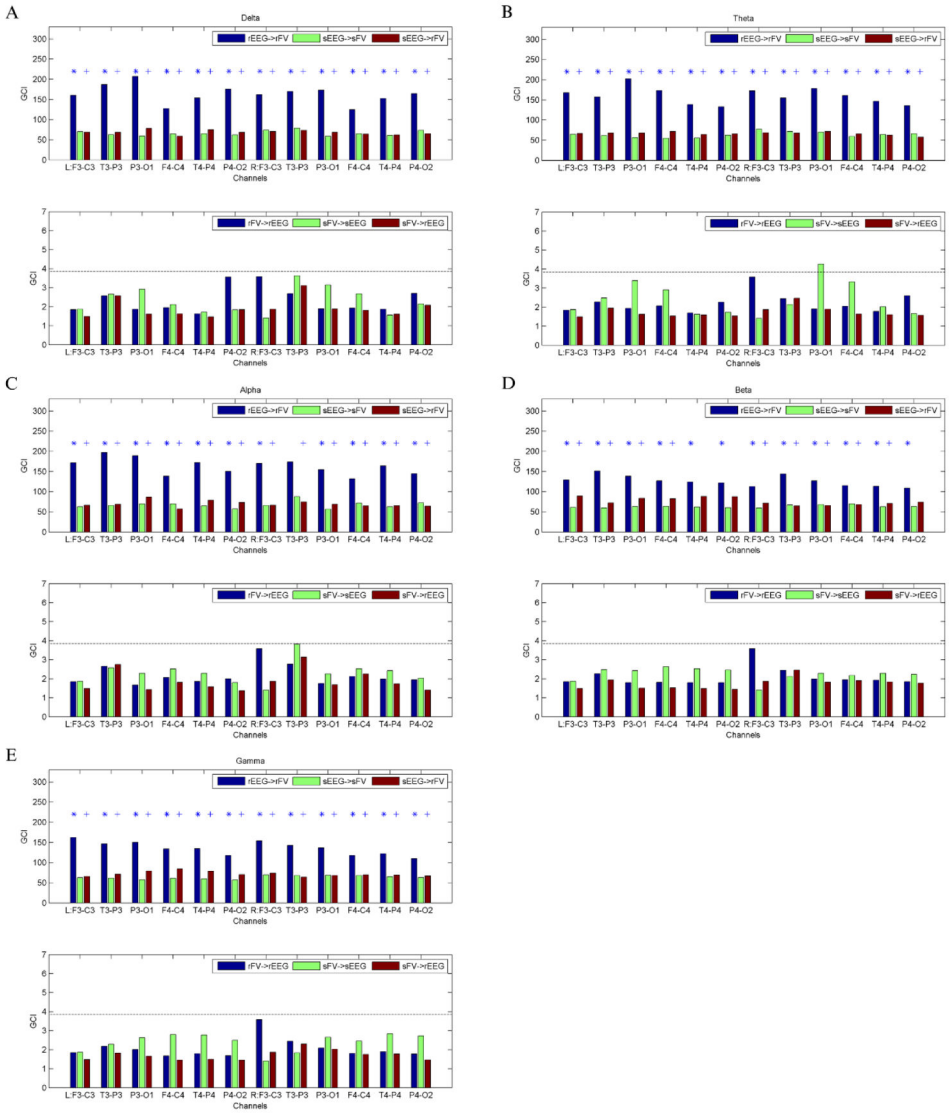

Figure 3.

Comparison between the GCI values in surrogate and original recording datasets. GCI values of surrogate data (green bar for both surrogate EEG and FV, red bar for surrogate EEG and raw FV) are significantly lower than GCI values of the raw data (blue bar) in the direction of EEG→FV in (A) Delta band, (B) Theta band, (C) Alpha band, (D) Beta band, and (E) Gamma band (upper panel in each subfigure). However, no significant difference exists between the GCI of real data and surrogate data in the inverse direction (FV→EEG) (Lower panel of each subgraph). The dash line represents the significant causality threshold. GCI: Granger causality Index. FV: cerebral blood flow velocity. rEEG: raw EEG, rFV: raw FV, sEEG: surrogate EEG, sFV: surrogate FV. * means significant difference between rEEG→rFV and sEEG→sFV, and + means significant difference between rEEG→rFV and sEEG→rFV.

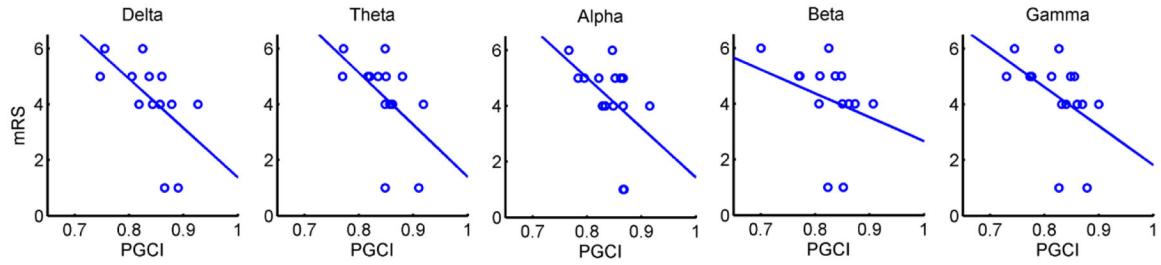

Figure 4.

Correlation plot between average PGCI and mRS (n = 15). GCI: Granger causality Index. mRS: modified Rankin Scale. PGCI: proportions of significant GCI.

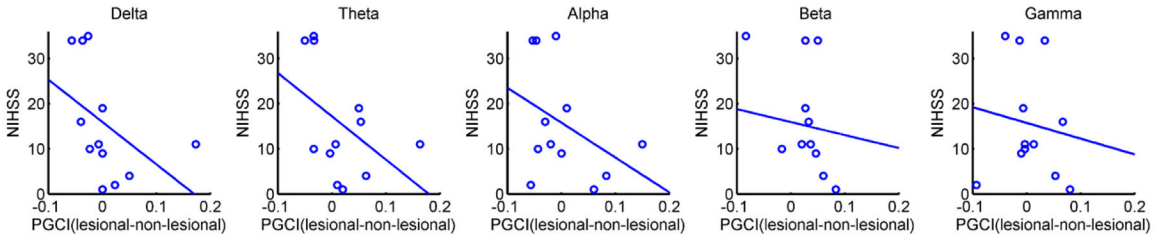

Figure 5.

Correlation plot between PGCI difference (left and right side) and discharge NIHSS (n = 14). NIHSS: NIH stroke scale.

Table 1

Patient demographics

Patient	Sex	Stroke Arterial Territory	Age	NIHSS at discharge	mRS at discharge
1	M	RICA	57	10	4
2	M	LICA	75	19	5
3	F	BA	64	35	5
4	M	BA	61	NA	NA
5	M	BA	45	NA	NA
6	F	LICA	85	NA	6
7	M	RICA	54	34	5
8	M	BA	46	10	5
9	M	LICA	56	4	4
10	M	LICA	62	11	4
11	F	LICA	68	11	4
12	M	RICA	58	9	4
13	M	LMCA	66	1	1
14	M	RICA	76	35	6
15	M	LMCA	62	34	5
16	F	RICA	56	2	1
17	M	RMCA	57	16	5

NIHSS: NIH stroke scale; mRS: Modified Rankin Scale for neurologic disability, NA: not available. ICA: internal carotid artery, MCA: middle cerebral artery, BA: basilar artery (BA).

Table 2

Average proportions of 5-min windows with significant GCI from EEG→FV, FV→EEG, surrogate EEG (sEEG) → FV and from surrogate FV (sFV) →EEG.

EEG Frequency Band	EEG→FV (Mean±SD)	FV→EEG (Mean±SD)	sEEG→FV (Mean±SD)	sFV→EEG (Mean±SD)
Delta	0.84 ± 0.08	0.11 ± 0.14	0.76±0.13	0.09±0.13
Theta	0.85 ± 0.08	0.11 ± 0.12	0.77±0.12	0.09±0.11
Alpha	0.85 ± 0.07	0.11 ± 0.12	0.77±0.12	0.09±0.12
Beta	0.82 ± 0.08	0.10 ± 0.11	0.75±0.14	0.09±0.11
Gamma	0.83 ± 0.08	0.10 ± 0.10	0.76±0.13	0.09±0.11

Table 3.

The correlation coefficient (R) and p value of the proportions of significant PGCI and mRS.

R, p	Delta	Theta	Alpha	Beta	Gamma
F3-C3→FVL	[−0.44, 0.10]	[−0.28, 0.31]	[−0.22, 0.44]	[−0.37, 0.18]	**[−0.76, 0.00]***
T3-P3→FVL	**[−0.61, 0.02]***	[−0.40, 0.14]	**[−0.63, 0.01]***	[−0.49, 0.06]	[−0.22, 0.42]
P3-O1→FVL	[−0.07, 0.81]	**[−0.66, 0.01]***	[−0.06, 0.83]	[−0.48, 0.07]	**[−0.68, 0.01]***
F4-C4→FVL	[−0.03, 0.92]	[−0.22, 0.44]	[−0.18, 0.52]	**[−0.78, 0.00]***	**[−0.66, 0.01]***
T4-P4→FVL	[−0.14, 0.61]	[−0.17, 0.55]	[0.07, 0.81]	**[−0.62, 0.01]***	**[−0.74, 0.00]***
P4-O2→FVL	[−0.38, 0.16]	[−0.26, 0.34]	[−0.15, 0.60]	**[−0.59, 0.02]***	[−0.07, 0.81]
F3-C3→FVR	[−0.48, 0.07]	[−0.13, 0.65]	[−0.43, 0.11]	[−0.08, 0.76]	[−0.35, 0.20]
T3-P3→FVR	[−0.48, 0.07]	[−0.34, 0.21]	**[−0.45, 0.09]***	[−0.28, 0.31]	[−0.34, 0.21]
P3-O1→FVR	**[−0.56, 0.03]***	[−0.40, 0.14]	[−0.08, 0.77]	[−0.42, 0.11]	[−0.23, 0.41]
F4-C4→FVR	[−0.25, 0.36]	[−0.42, 0.12]	**[−0.53, 0.04]***	[−0.32, 0.25]	[−0.16, 0.56]
T4-P4→FVR	[−0.26, 0.35]	[−0.47, 0.07]	**[−0.53, 0.04]***	[−0.20, 0.49]	[−0.41, 0.13]
P4-O2→FVR	**[−0.87, 0.00]***	[−0.46, 0.08]	[0.13, 0.64]	[−0.10, 0.72]	[−0.06, 0.83]
Average	**[−0.71, 0.00]***	**[−0.59, 0.02]***	**[−0.59, 0.02]***	**[−0.57, 0.03]***	**[−0.62, 0.01]***
PGCI bilateral difference	[0.42, 0.12]	[0.40, 0.14]	[0.24, 0.40]	[−0.10, 0.73]	[0.10, 0.72]

Mark * means a significant correlation between PGCI and mRS.

Table 4.

The correlation coefficient (R) and p value of the PGCI and NIHSS at discharge.

R, p	Delta	Theta	Alpha	Beta	Gamma
F3-C3→FVL	[−0.28, 0.33]	[−0.42, 0.14]	[−0.23, 0.42]	[−0.14, 0.62]	[−0.69, 0.01]
T3-P3→FVL	[−0.32, 0.26]	[−0.39, 0.17]	[−0.36, 0.20]	[−0.46, 0.09]	[−0.10, 0.73]
P3-O1→FVL	[−0.08, 0.79]	**[−0.61, 0.02]***	[0.19, 0.51]	[−0.32, 0.27]	[−0.48, 0.08]
F4-C4→FVL	[0.11, 0.71]	[−0.22, 0.45]	[−0.17, 0.57]	**[−0.71, 0.00]***	**[−0.61, 0.02]***
T4-P4→FVL	[−0.17, 0.56]	[−0.12, 0.67]	[0.41, 0.15]	**[−0.55, 0.04]***	**[−0.64, 0.01]***
P4-O2→FVL	[−0.33, 0.24]	[0.00, 0.99]	[−0.33, 0.24]	**[−0.55, 0.04]***	[0.06, 0.85]
F3-C3→FVR	[−0.33, 0.24]	[−0.10, 0.73]	[−0.14, 0.63]	[0.23, 0.42]	[−0.12, 0.67]
T3-P3→FVR	[−0.42, 0.13]	[−0.28, 0.34]	[−0.38, 0.18]	[−0.21, 0.47]	[−0.27, 0.34]
P3-O1→FVR	**[−0.69, 0.01]***	[−0.37, 0.19]	[0.02, 0.94]	[−0.19, 0.51]	[0.02, 0.94]
F4-C4→FVR	[−0.27, 0.35]	[−0.53, 0.05]	[−0.29, 0.31]	[−0.07, 0.82]	[0.10, 0.73]
T4-P4→FVR	[−0.02, 0.95]	[−0.24, 0.42]	[−0.42, 0.14]	[0.14, 0.63]	[−0.12, 0.68]
P4-O2→FVR	**[−0.66, 0.01]***	[−0.28, 0.34]	[0.25, 0.38]	[0.31, 0.28]	[0.19, 0.52]
Average	**[−0.56, 0.04]***	[−0.46, 0.10]	[−0.35, 0.23]	[−0.34, 0.24]	[−0.43, 0.12]
PGCI bilateral difference	**[−0.68, 0.01]***	[−0.44, 0.15]	[−0.25, 0.43]	[−0.28, 0.38]	[−0.26, 0.41]

Mark * means a significant correlation between PGCI and NIHSS.